In situ passivation of GaAsP nanowires — **Source link**

C. Himwas, Stéphane Collin, P. Rale, Nicolas Chauvin ...+6 more authors

Institutions: Université Paris-Saclay, Institut des Nanotechnologies de Lyon

Related papers:

- InP Nanowire Array Solar Cells Achieving 13.8% Efficiency by Exceeding the Ray Optics Limit

- A GaAs Nanowire Array Solar Cell With 15.3% Efficiency at 1 Sun

- Effect of the GaAsP shell on optical properties of self-catalyzed GaAs nanowires grown on silicon

- Surface-passivated GaAsP single-nanowire solar cells exceeding 10% efficiency grown on silicon.

- Self-catalyzed ternary core-shell GaAsP nanowire arrays grown on patterned Si substrates by molecular beam epitaxy.

In situ passivation of GaAsP nanowires

C. Himwas, S. Collin, P. Rale, Nicolas Chauvin, G. Patriarche, F. Oehler, F H
Julien, L. Travers, J-C Harmand, Maria Tchernycheva

In-situ passivation of GaAsP nanowires

C. Himwas[1], S. Collin[2], P. Rale[2], N. Chauvin[3], G. Patriarche[2], F. Oehler[2], F. H. Julien[1], L. Travers[2], J.-C. Harmand[2], M. Tchernycheva[1]

[1] *Centre de Nanosciences et de Nanotechnologies – site Orsay, UMR 9001 CNRS, Univ. Paris Sud, Univ. Paris-Saclay, Bat 220, rue André Ampère, 91405 Orsay, France*

[2] *Centre de Nanosciences et de Nanotechnologies – site Marcoussis, UMR 9001 CNRS, Univ. Paris Sud, Univ. Paris-Saclay, Route de Nozay, 91460 Marcoussis, France*

[3] *Université de Lyon, Institut des Nanotechnologies de Lyon (INL), UMR 5270CNRS, INSA-Lyon, 7 avenue Jean Capelle, 6962 Villeurbanne, France*

Abstract

We report on the structural and optical properties of GaAsP nanowires (NWs) grown by molecular-beam epitaxy. By adjusting the alloy composition in the NWs, the transition energy was tuned to the optimal value required for tandem III-V/silicon solar cells. We discovered that an unintentional shell was also formed during the GaAsP NW growth. The NW surface was passivated by an in-situ deposition of a radial Ga(As)P shell. Different shell compositions and thicknesses were investigated. We demonstrate that the optimal passivation conditions for GaAsP NWs (with a gap of 1.78 eV) are obtained with a 6 nm-thick GaP shell. This passivation enhances the luminescence intensity of the NWs by 2 orders of magnitude and yields a longer luminescence decay. The luminescence dynamics changes from single exponential decay with a 4 ps characteristic time in non-passivated NWs to a bi-exponential decay with characteristic times of 85 ps and 540 ps in NWs with GaP shell passivation.

1. Introduction

Solar energy conversion is now recognized as a serious candidate to replace the existing electricity production streams. Today, the record in conversion efficiency is detained by multi-junction solar cells based on III-V semiconductors.[1] However, the wide adoption of these devices is hindered by their high production cost, to a large extent due to the expensive III-V substrates. In addition, to achieve a high conversion efficiency of the solar spectrum in a III-V tandem or multi-junction cell, a stacking of lattice-mismatched materials is required.

In a tandem device, the requirement of lattice-matching can be avoided using nanowires (NWs). The NW diameter is small enough, the III-V NWs can be grown on lattice-mismatched substrates without forming dislocations, thanks to the strain relaxation through the free lateral surface.[2] NW arrays also have very attractive optical properties such as a small optical reflectance and enhanced light diffusion, leading to an increased absorption in comparison to thin films.[3,4] Nowadays, a number of NW-based single junction photovoltaic (PV) demonstrators have been built[5–7] with a record efficiency of 15.3% for bottom-up GaAs NWs[6], 17.8% for InP top-down NWs.[7]

Although the above examples have been obtained using relatively expensive III-V substrates, there may be a benefit to adopt a hybrid geometry which combines a 2D Si bottom cell with a NW top cell in a tandem device. This approach, proposed by LaPierre *et al*.,[8] necessitates smaller amounts of expensive III-V materials compared to conventional III-V tandem cells, furthermore standard back contacting procedures of the mature Si PV manufacturing technology can be used.

Since the optimal III-V band gap to be combined with Si in a tandem cell lies around 1.7 eV,[6] there is a strong incentive to obtain NWs with a direct band gap close to this value

using III-V ternary alloys such as InGaP[9,10] or GaAsP.[11–13] In balance with their above-mentioned advantages, NWs are very sensitive to surface states because of their large surface-to-volume ratio. These surface states can act as recombination centers for photo-generated carriers and thus induce losses which can be particularly severe in III-As materials because of their high surface recombination velocity (SRV).[14,15]

The impact of surface states can be minimized by surface passivation. This can be done by adding a passivation layer made of wider band gap semiconductor. Its thickness must be large enough to prevent minority carriers to access the NW surface states, but it should not exceed a critical value resulting in plastic relaxation due to the lattice-mismatch. While numerous studies concern the growth of binary compound NWs and their surface passivation,[14–19] there are only few reports on the growth of self-catalyzed GaAsP NWs[11,12] and only one report mentioning their passivation by an InGaP shell.[12]

In this work, we synthesize GaAsP NWs in a broad range of compositions, and we optimize their in-situ passivation. We adjust the GaAsP composition to tune the band gap to the 1.7 – 1.8 eV range, which is relevant for efficient III-V NW/Si tandem devices. During the GaAsP NWs growth by molecular-beam epitaxy (MBE), we found for the first time, that unintentional GaAsP shells were simultaneously formed with a comparatively lower P concentration. To reduce surface recombination losses of the GaAsP NWs, in-situ passivation with an epitaxial overgrowth of a GaAsP shell of various P concentrations and thicknesses was investigated using photoluminescence (PL), time-resolved (TR)-PL, and cathodoluminescence (CL) techniques. We show that a 200 times enhancement of the luminescence intensity and a slower luminescence decay is achieved for the optimized 6 nm-thick GaP shell passivation.

2. Experimental Details

Prior to the growth, Si(111) substrates were chemically etched by diluted HF 5% for 2 min in order to completely remove the native SiO_x from the surfaces. A controlled SiO_x was then formed using a 1-min oxygen plasma treatment. This procedure was applied to obtain a reproducible SiO_x layer at the surface since it critically influences the nucleation of NWs.[20] Subsequently, the substrates were outgassed in ultra-high vacuum (UHV) at 450 °C for 1 hour. The growth of GaAsP NWs was carried out by solid-source molecular beam epitaxy (MBE) on intrinsic Si(111) substrates at 610°C for 30 min. It proceeded by vapor-liquid-solid (VLS) mechanism catalyzed by Ga droplets, so called self-catalyzed growth. Ga flux was set equivalent to a two-dimensional deposition rate on GaAs (001) of 0.2 nm·s^{-1} calibrated from reflection high-energy electron diffraction oscillations. As and P were supplied by solid-source cells, equipped with individual valves and shutters and producing As_4 (or As_2 depending on the cracker temperature) and P_2 molecules. V/III beam equivalent pressure (BEP) ratios were set at 10 – 12. Due to the different gauge sensitivities among elements, the P/(P+As) BEP ratio, defined as $\varepsilon_P = BEP_P/(BEP_P+BEP_{As})$, is not an actual P concentration in the vapor phase. However, it varies consistently with the actual P concentration, hence it can be used as an experimental parameter. In our experiment, ε_P was consecutively adjusted to 0.10, 0.20, 0.25, and 0.33.

For the GaAsP/Ga(As)P core/shell structures, the growth process was the following: (1) GaAsP core synthesis by self-catalyzed VLS, (2) Ga droplet crystallization, and (3) Ga(As)P shell radial overgrowth. The crystallization process was performed by exposing GaAsP NWs to P and As fluxes (closing only the Ga shutter) during 5 min while maintaining the substrate temperature at 610°C. During this step, Ga droplets were consumed by developing a NW extremity with inclined crystallographic planes. (More details about the crystal structure of

the NW extremity will be further given in Figure 3). After the catalyst crystallization, the substrate temperature was decreased to ~500°C for the shell growth. The absence of catalyst and the low substrate temperature are favorable to radial growth and thus enable the shell formation.[21,22] For the GaAsP shell case, the As cracker temperature was also increased to ~900°C, in order to crack As_4 into As_2 molecules which was shown to enhance the lateral deposition.[29] After stabilizing the substrate temperature, the Ga(As)P shell was deposited by opening the Ga, As, and P shutters simultaneously. Two shell concentrations and various thicknesses were tested (while maintaining all the prior steps unchanged). During the shell deposition, Ga flux and V/III BEP ratio were kept identical to those used for the NW growth and the ε_P was adjusted to 0.40 and 1.00. The shell deposition time for the GaP case was varied between 0 and 5 min, resulting in a set of samples with shell thicknesses between 0 and 14 nm. The structure of the analyzed samples is summarized in Tables I and II.

The morphology of the NWs was first observed in a scanning electron microscope (SEM). Their structure was further analyzed by transmission electron microscopy (TEM) and by scanning transmission electron microscopy (STEM) in high-angle annular dark field (HAADF) mode. The optical characterization of the samples was performed by PL and CL. PL spectra were obtained by exciting the NWs with a continuous-wave Ar^{2+} laser (λ=514 nm) with a power density in the range of 1-100 W/cm^2. The emission from the sample was collected by a Jobin Yvon HR460 monochromator equipped with a charge-coupled device (CCD) camera. The time-resolved (TR-) PL was measured by exciting the NWs with a 515 nm pulsed laser with a 54 MHz repetition rate and a 200 fs pulse duration. The luminescence was collected using a streak camera coupled to a monochromator enabling a 5 ps time resolution. Continuous CL measurements were performed in an Attolight Chronos cathodoluminescence microscope,[24] using an acceleration voltage of 5-10 kV and an impinging current of 0.5-1 nA. The sample emission was collected by an achromatic

reflective objective and dispersed by a Jobin Yvon iHR320 monochromator equipped with a CCD camera.

3. Results and discussion

In this section, the structural and optical properties of the GaAsP NW cores are first described. Then the modifications induced by the Ga(As)P shell radial overgrowth are discussed and the optimal passivation conditions are derived.

3.1 GaAs$_{1-x}$P$_x$ core NWs

First, we analyze the structural and optical properties of GaAs$_{1-x}$P$_x$ NWs without droplet crystallization and shell with a range of P concentrations (x_{solid}) corresponding to a direct band gap close to 1.7-1.8 eV. These elements represent a prerequisite study for demonstrating the NW passivation conditions discussed in the next section. 4 samples, referred to as C1, C2, C3, and C4, were synthesized with different ε_P, namely 0.10, 0.20, 0.25, and 0.33 respectively (Table I).

| Sample	Growth conditions: GaAsP core		$E_{PL, RT}$ (eV)	P concentration (x_{solid})
	P/(P+As) BEP ratio (ε_P)	V/III BEP ratio		
C1	0.10		1.67	0.21
C2	0.20	10	1.78	0.30
C3	0.25		1.85	0.36
C4	0.33		-	-

Table I: Description of the GaAsP NWs samples: P/(P+As) beam equivalent pressure ratio (ε_P), V/III beam equivalent pressure ratio, room temperature peak emission energy ($E_{PL,RT}$ (eV)), and P concentration (x_{solid}) calculated using Eq.(1).
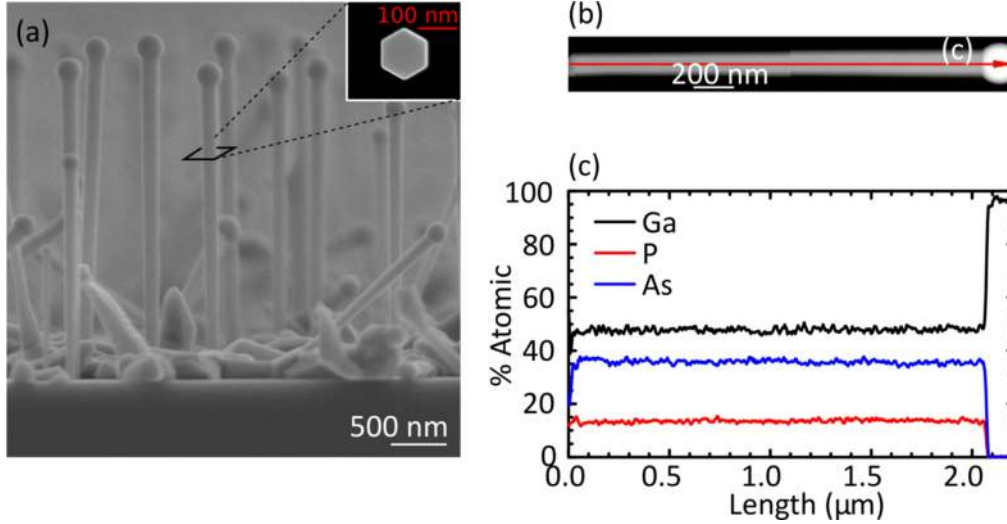
FIG. 1. (a) 90°-tilted SEM image of GaAsP NWs grown on Si(111) (sample-C2). The inset shows a top view image illustrating the wire hexagonal shape limited by six {110}-type sidewalls. (b) STEM image of a NW from sample-C2, red-arrow shows the direction of the EDX line-scans presented in panels c. (c) EDX profile for elements Ga, P, and As performed along the growth axis.

Figure 1(a) depicts the SEM image of GaAsP NWs grown with ε_P = 0.20 (sample-C2). The density of nanowires is 1-2 wire/μm^2, with a typical percentage of vertically-growing NWs of 60%. The average NW diameter is 140 nm and the length is 2-3 μm. Ga droplets with a high contact angle can be observed at the wire tips, similar to the case of self-catalyzed GaAs NWs,[25] and GaP NWs.[26] Such nanowires possess a hexagonal shape limited by six {110} sidewalls as shown in the inset of Fig. 1(a). In order to probe the compositional profile of the GaAsP NWs, the energy-dispersive X-ray spectroscopy (EDX) measurements were performed in STEM mode (demonstrated in Fig. 1(b)). Atomic percentages of each element (Ga, As, and P) were extracted along the growth axis of the NW (Fig. 1(c)). The compositional profile shows that the GaAsP NW possesses a P concentration, x_{solid} = 0.28±0.02.
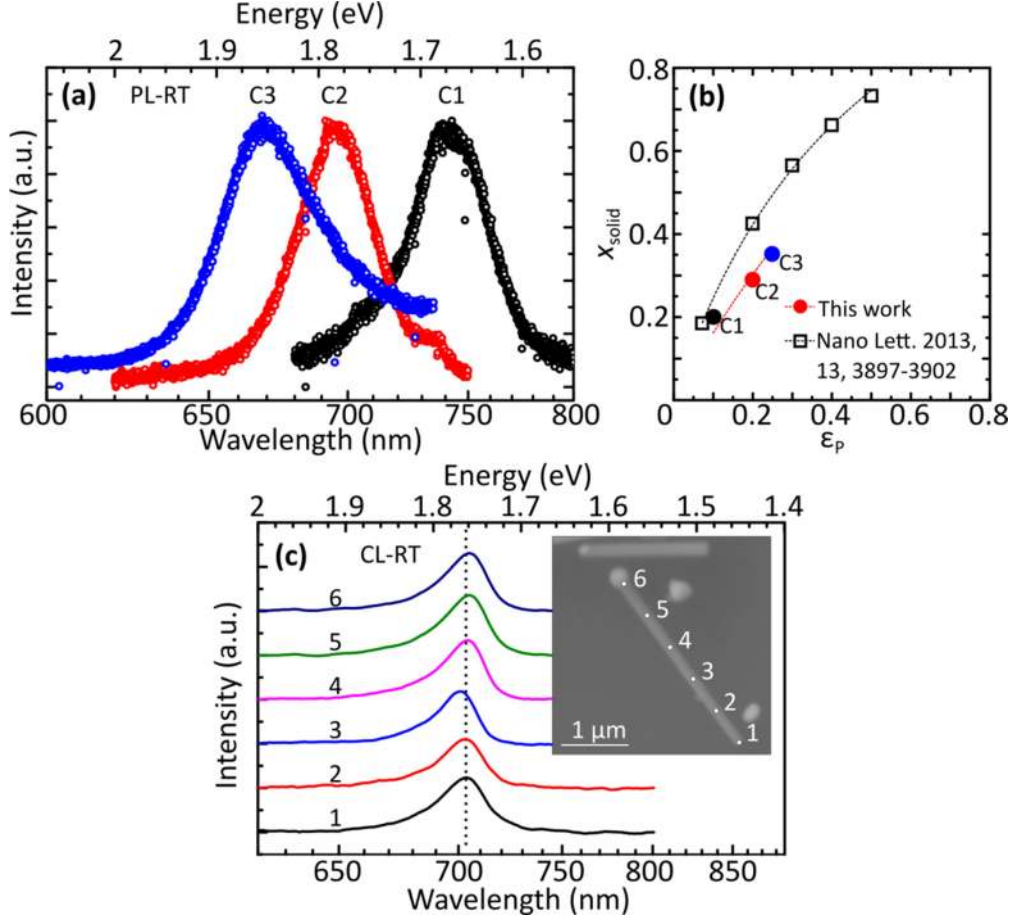
FIG. 2. (a) Normalized RT PL spectra of GaAsP NWs for samples-C1, C2, and C3. (b) Calculated P concentrations (x_{solid}) (from PL peak energy) versus P/(P+As) BEP ratios (ε_P). The hollow squares show the evolution of x_{solid} (from EDX measurements) as a function of ε_P from the literature.[11] (c) RT CL spectra for a single GaAs$_{0.70}$P$_{0.30}$ NW (sample-C2) obtained for different excitation positions from the bottom to the top. The inset shows SEM image of the wire collected during CL acquisition showing the excitation positions.

Figure 2(a) shows the room temperature (RT) PL spectra of GaAsP NW ensembles. In these macro-PL experiments, the signal averages the emission of a large number of NWs (approximately $10^3 - 10^4$ wires accounting for a laser spot of ~100 μm). The peak emission energy is blue-shifted from 1.67 to 1.85 eV when changing ε_P from 0.10 to 0.25. The luminescence of GaAsP NWs grown with $\varepsilon_P = 0.33$ could not be observed, possibly due to an indirect bandgap (X valley of the conduction band) of this P-rich sample. The peak energies extracted from the PL measurements were used to derive the composition of the alloy (x_{solid}). We assume the following quadratic dependence

$$E_{g,GaAs_{1-x}P_x} = (1-x)\cdot E_g(GaAs) + (x)\, E_g(GaP) - bx\cdot(1-x) \qquad (1)$$

reported for ZB GaAsP[33,34] where b is the bowing parameter taken equal to 0.19.[33] This approach to estimate x_{solid} is validated by the good agreement with the EDX measurements for sample-C2, for which both methods yield $x_{solid} \sim 0.30$. The relation between the solid P concentration and ε_P is presented in Fig. 2(b) and can be described by the equation:

$$x_{solid} = (R \cdot \varepsilon_P)/(1 + (R-1) \cdot \varepsilon_P) \tag{2}$$

where R is a fitting parameter including the P-to-As incorporation ratio and the difference in gauge sensitivity. The equation (2) fits our experimental results for R equal to 1.73. The value of R is larger than unity, which is in agreement with the report of Zhang et $al.$ [11] who obtained an even higher value of R equal to 2.97 (cf. Fig 2b). It is noteworthy that the VLS incorporation rate (group V limited) is different from the planar epitaxial growth (group III limited), for which As is more easily incorporated in the solid than P.[35–37] We note here that in Ref. 11 the authors grow multiple segments of GaAsP consecutively increasing the P concentration along the growth axis and then extract the R value from the EDX data. As we show below, an unintentional GaAsP shell is simultaneously formed during the GaAsP nanowire growth (see discussion of Figure 4). Therefore, this unintentional shell may disturb the interpretation of the P-core concentration measured by EDX especially at the bottom part of the wire. The P-to-As incorporation ratio is needed to be extracted taking this effect into account, which has not been done in Ref 11. This may explain the difference with the R value we have obtained. We note that in our case, sample-C2 exhibits a peak emission energy at 1.78 eV, a value which is well-suited for a III-V NW/Si tandem solar cell. This sample was selected for further investigations by CL.

NWs from sample-C2 were dispersed on a Si carrier substrate for CL analyses of individual NWs. Figure 2(c) shows RT CL emission spectra for different positions (labelled 1 to 6 and indicated in the SEM image (inset of Fig. 2(c))). From the bottom to the top of the

NW, the CL spectra are peaked at 1.77 eV. The PL and CL peak energies are in agreement with the P concentration, x_{solid} = 0.28±0.02 extracted from the EDX studies (Fig. 1(c)). However, PL spectra exhibit a larger luminescence linewidth (~100 meV) than CL spectra (~60 meV). This increase of the broadening can be attributed to the spread of nanowire compositions within the large ensemble probed by PL.

3.2 GaAs$_{0.72}$P$_{0.28}$/Ga(As)P core/shell NWs

In the following, we have fixed the alloy composition yielding the desired emission energy (x_{solid} ~ 0.30) and we explore the growth conditions of the shell in order to minimize the surface recombination losses. As mentioned before, prior to the shell deposition, Ga catalyst droplets were consumed and the substrate temperature was lowered to ~500°C in order to inhibit the axial growth. Different shells were analyzed (Table II). The aim was to obtain a shell with a band gap higher than the core band gap. In order to limit the core/shell lattice-mismatch and to prevent the plastic relaxation of the shell, we first investigate a shell growth condition with a moderate P/(P+As) BEP ratio (ε_P = 0.4). Then, we investigate a GaP shell with various thicknesses in order to evaluate the impact of lattice mismatch-induced strain. GaP shells of 0, 2.8, 5.6, 8.4, and 14 nm were obtained by increasing the shell deposition time from 0 to 5 min. After the growth, the structural characterizations were performed by TEM or high-resolution STEM while the optical quality of each sample was asserted by PL.

Different shell composition

Sample	GaAsP core		Ga(As)P shell		Shell deposition time (min)	$E_{PL, RT}$ (eV)
	ε_P	x_{solid}	ε_P	x_{solid}		
CS1			-	-	0	1.74
CS2	0.19	0.27	-	-	0	1.74
CS3			0.40	0.27	2	1.72
CS4			1.00	1.00	2	1.79

Sample-CS1: $GaAs_{0.73}P_{0.27}$ nanowires, CS2 crystallized-droplet $GaAs_{0.73}P_{0.27}$ nanowires, CS3 $GaAs_{0.73}P_{0.27}/GaAs_{0.73}P_{0.27}$ core/shell nanowires, and CS4 $GaAs_{0.73}P_{0.27}/GaP$ core/shell nanowires.

Different shell thickness

Sample	GaAsP core		GaP shell		Shell deposition time (min)	$E_{PL, RT}$ (eV)
	ε_P	x_{solid}	ε_P	x_{solid}		
0 nm					0	1.76
2.8 nm					1	1.75
5.6 nm	0.20	0.28	1.00	1.00	2	1.75
8.4 nm					3	1.81
14 nm					5	1.85

Table II: Description of the GaAsP/Ga(As)P core/shell NW samples: P/(P+As) beam equivalent pressure ratio (ε_P) for the core, P concentration (x_{solid}) for the core, ε_P for the shell, x_{solid} for the shell, shell deposition time, and RT peak emission energy ($E_{PL,RT}$ (eV)).

Ga droplet crystallization NWs (sample-CS2) were selected to be structurally characterized by TEM in order to investigate the difference of the nanowire structure grown during the catalyst consumption and the nanowire stem.
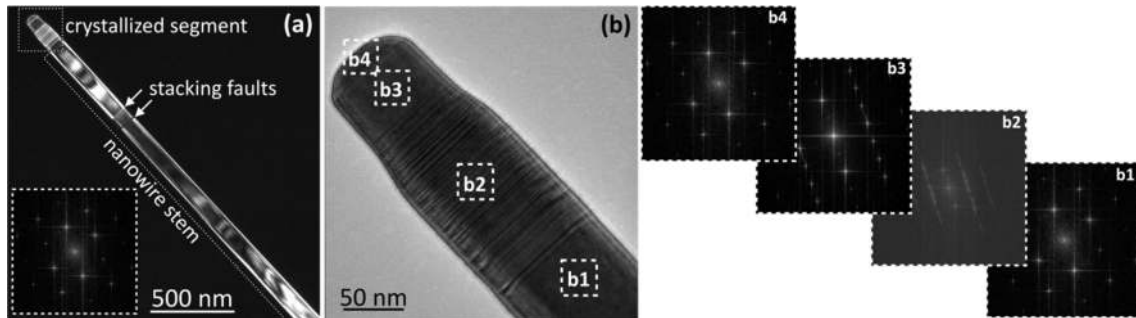
FIG. 3. (a) TEM image of crystallized GaAsP NW (sample-CS2). The inset shows FFT image performed at the nanowire stem revealing ZB structure. (b) Zoomed TEM micrograph of crystallized GaAsP NW (sample-CS2) taken at the nanowire tip, where the crystallization process took place, showing various phases at different regions. (b1)-(b4) FFT images performed at different positions of (b), revealing ZB structure (b1), polytypic phase region (b2), WZ structure (b3), and ZB structure (b4).

Figure 3(a) illustrates the TEM image of sample-CS2. Only 2 twin planes (white arrows) were observed over 2 micron-long nanowire. The GaAsP NWs crystallized with zinc-blende (ZB) structure are identified by fast Fourier transform (FFT) (inset of Fig.3(a)).

Figure 3(b) shows the TEM micrograph taken at the nanowire tip of sample-CS2 corresponding to the segment grown during the catalyst consumption. This segment possesses different crystal phases which are identified by FFT. In the lower region (Fig. 3(b1)), the NW has ZB structure which is a dominant structure for the GaAsP NWs. Moving towards the tip where growth proceeded during the catalyst consumption, the NW acquires a polytypic structure (Fig.3(b2)). In addition to the crystal phase change, a decrease of the NW diameter was also observed in this region. Further decrease of the catalyst volume results in the stabilization of the wurtzite (WZ) structure (Fig. 3(b3)), and finally it returns to a ZB structure at the topmost position (Fig. 3(b4)). The sequence of structural and morphological modifications of the GaAsP NWs which occur during the catalyst consumption is similar to those reported for binary GaAs NWs.[27–31] It has been shown that the volume and contact angle of the catalyst droplet play an important role on the modifications.[27,32]
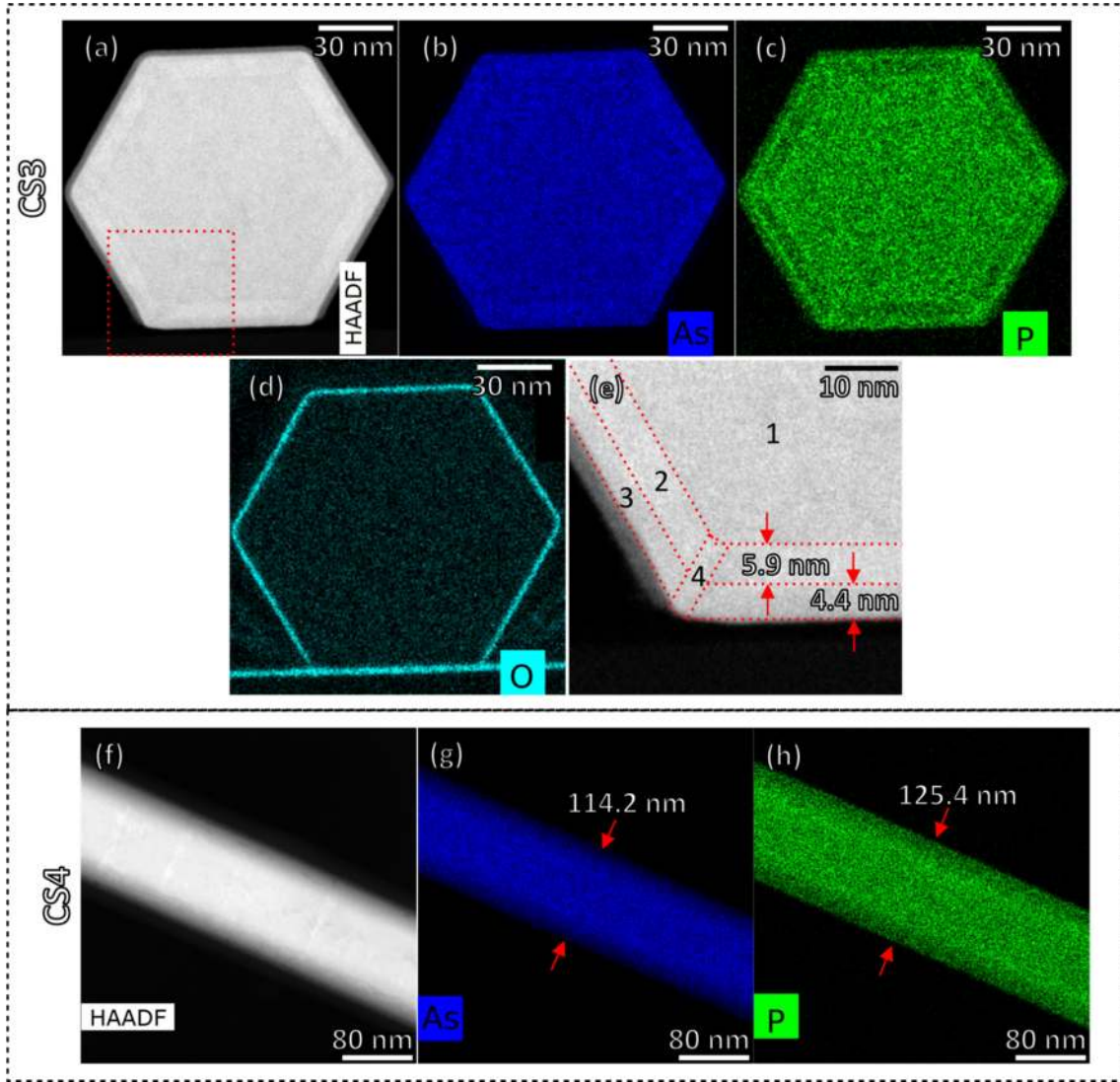
FIG. 4 (a) Cross-sectional HAADF-STEM micrograph of GaAsP/GaAsP core/shell NW lying on a substrate (sample-CS3). (b)-(d) Associated EDX mappings performed on sample-CS3 in STEM mode, showing As, P, and O element. (e) Zoomed cross-sectional HAADF-STEM micrograph of sample-CS3. Delimited areas marked as "1", "2", "3", and "4" have the P concentration (x_{solid}) of 0.27, 0.22, 0.27, and 0.32, respectively. (f) HAADF-STEM micrograph of GaAsP/GaP core/shell NW (sample-CS4). (g)-(h) Associated EDX mappings performed in STEM mode, showing As, and P element.

Figure 4(a) shows the cross-sectional HAADF-STEM micrograph of a GaAsP/GaAsP core/shell NW (sample-CS3) lying on a carrier substrate at the bottom of the image. EDX maps for As, P, and O elements are shown in Fig. 4(b), (c) and (d), respectively. The bottom left corner of the NW is magnified in Fig. 4(e). From center to periphery, complex and faint contrasts are observed, revealing a double shell heterostructure. Areas marked as "1", "2", "3", and "4" have a P concentration equal to 0.27, 0.22, 0.27, and 0.32 respectively. The GaAs$_{0.73}$P$_{0.27}$ core is surrounded by a first 5.9 nm-thick GaAs$_{0.78}$P$_{0.22}$ shell (zone 2) which

was non-intentionally formed during the growth of the core. Its thickness is not uniform and changes along the wire. More details about the unintentional shell properties can be found in *supporting information* S1. The second 4.4 nm-thick GaAs$_{0.73}$P$_{0.27}$ shell (zone 3) corresponds to the intentional passivating shell.

GaAsP intentional shell in sample-CS3 was aimed to possess a moderate P concentration (the shell was grown with ε_P = 0.40). From the EDX result, the intentional GaAsP shell possesses x_{solid} = 0.27. By applying equation (2), this experimental result can be fitted with R equal to 0.55. Contrary to the GaAsP core case, this value is lower than unity which is similar to the situation of planar epitaxial growth,[35–37] suggesting that As is possibly more favourable than P in this growth condition. However, the direct comparison between VLS and VS growth mechanisms is hindered by the different growth temperatures, and different gauge sensitivities between As$_4$ (used during VLS growth), and As$_2$ (used during VS growth).

In addition, we note that the P incorporation is more favourable at the corners of the hexagonal NW cross section (zone 4 of Fig. 4(e)). The P concentration in this region is, x_{solid} = 0.32, slightly higher than in the core, and in the rest of the shell. Modulation of the concentration at the corners of hexagonal NWs was already reported for ternary shells consisting of two group III elements: Al-rich corners were observed in AlGaAs[38] or AlInP[39,40] shells, and ternary shells consisting of two group V elements: P rich corners were also observed in GaAsP.[41]

For GaP shell (sample-CS4), the HAADF-STEM micrograph was taken along the wire axis (Fig. 4(f)). EDX mappings of As, and P elements (Fig. 4(g), and (h)) were performed in STEM mode. The As-containing diameter (i.e. the core diameter), and P-containing diameter (i.e. the whole NW diameter) were measured equal to 114.2, and 125.4 nm, respectively.

Hence, the GaP shell is 5.6 nm-thick. The direct EDX measurement 0.37±0.05 averaging over the GaAsP/GaP core/shell structure, can be corrected to obtain the P content of the GaAsP core with ($x_{solid,core}$ = 0.26±0.05). Note that this value averages the composition of the thin unintentional shell (previously evidenced in the cross-sectional analysis of sample-CS3) and the compostion of the GaAsP core. The obtained average value (x_{solid} = 0.26) is compatible with the 5.9 nm-thick unintentional shell (x_{solid} = 0.22) and the 45 nm-radius GaAsP core (x_{solid} = 0.27).
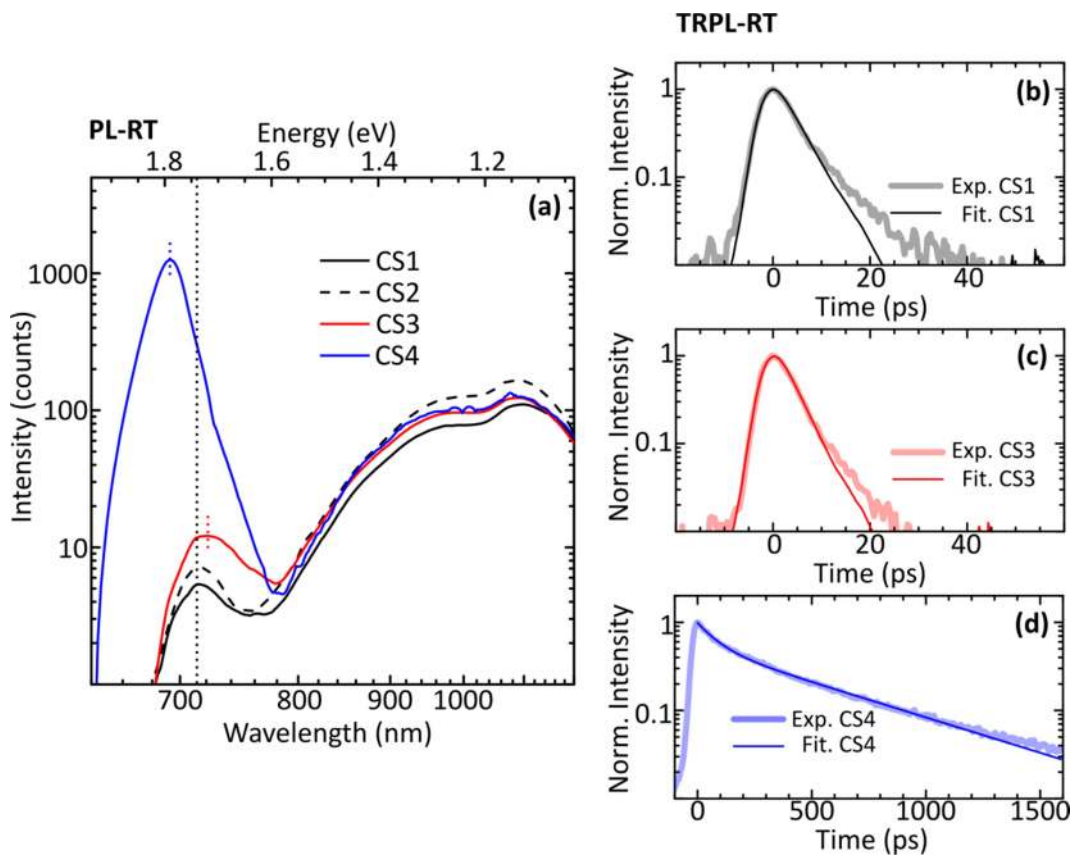
FIG. 5. (a) RT PL emission spectra of CS1, CS2, CS3, and CS4 NW ensembles. (b), (c), and (d) RT TR-PL decays and their fittings of CS1, CS3, and CS4.

Figure 5(a) shows RT PL spectra of NW ensembles for 4 samples, namely GaAs$_{0.73}$P$_{0.27}$ core NWs (CS1, black line), GaAs$_{0.73}$P$_{0.27}$ core NWs with crystallized-droplets (CS2, black dashed line), GaAs$_{0.73}$P$_{0.27}$/GaAs$_{0.73}$P$_{0.27}$ core/shell NWs (CS3, red line), and GaAs$_{0.74}$P$_{0.26}$/GaP core/shell NWs (CS4, blue line). In addition to the near band edge emission of the NWs (1.75-1.85 eV), broad spectral features (1.00-1.55 eV) are observed for

all the samples. These broad emission bands were absent in dispersed NWs luminescence (see *supporting Information* S2), therefore we attribute them to parasitic overgrowth on the substrate. CS1 and CS2 samples have similar spectra, showing that the droplet crystallization process does not affect the optical response of the NWs. Surface passivation with $GaAs_{0.73}P_{0.27}$ shell (CS3) enhances the integrated luminescence intensity by a factor of 2.5, whereas the GaP shell (CS4) brings a 200 times enhancement with respect to CS1.

For sample-CS3, in addition to the slight integrated intensity enhancement, the peak is red-shifted by 15 meV compared to the spectrum of $GaAs_{0.73}P_{0.27}$ core NWs. These effects could be associated with the presence of the unintentional $GaAs_{0.78}P_{0.22}$ shell that becomes optically active when the whole structure is passivated with the intentional shell of higher band gap material ($GaAs_{0.73}P_{0.27}$). For sample-CS4, the peak energy is located at 1.79 eV. It is blue-shifted from the calculated band gap of $GaAs_{0.73}P_{0.27}$ by ~50 meV, which can be explained by strain-induced band gap modification. Similar results were reported for GaAs NWs: Couto *et al.*[17] observed a 50 meV emission blue-shift when passivating GaAs NWs with a GaAsP shell. Pistol *et al.*[40] reported theoretical band structure calculations for the binary case of GaAs/GaP core/shell NWs as a function of the core and shell radii. Taking the core radius to total radius ratio of 0.90 (corresponding to our GaAsP/GaP core/shell sample), the theoretically predicted blue-shift of the GaAs core energy is 62 meV. This value is higher than our experimental observation in the $GaAs_{0.73}P_{0.27}$/GaP case since the lattice mismatch in the simulated case (GaAs core and GaP shell) is higher than that of experimental case ($GaAs_{0.73}P_{0.27}$ core and GaP shell).

To understand the recombination dynamics, the carrier lifetime in $GaAs_{0.73}P_{0.27}$ NWs (CS1), $GaAs_{0.73}P_{0.27}$/$GaAs_{0.73}P_{0.27}$ core/shell NWs (CS3), and $GaAs_{0.73}P_{0.27}$/GaP core/shell NWs (CS4) was measured by TR-PL at room temperature (Fig. 5(b)-(d)). After de-

convolution by the response function of the experimental setup, CS1 and CS3 NWs are found to have a fast exponential decay with a characteristic time of 4 ps while CS4 presents a different recombination dynamics, featuring a bi-exponential decay with characteristic times of 85 ps and 540 ps. Due to the small value of the GaAsP exciton binding energy at room temperature, the decay time is dominated by electron-hole pair recombination.

The fast decay time of CS1 is similar to the decay times observed for GaAsP NWs grown by aerotaxy (7–16 ps).[13] This could be related to a combination of several processes: carrier transfer towards localized states in the NW volume and recombination on surface states. By performing surface passivation, we assume that the main modification concerns the surface state dynamics. The decay time of CS3 is similar to CS1, which implies that the GaAs$_{0.73}$P$_{0.27}$ shell does not provide an efficient potential barrier to prevent the carriers from reaching the surface states. For CS4 the carrier lifetime is increased (85 ps), suggesting that the surface recombination dynamics was significantly reduced by the GaP shell passivation.

After the fast decay component, sample-CS4 shows a slow decay component (540 ps), which may be attributed to non-radiative recombination of carriers in the NW volume, most probably due to the indirect carrier transitions in the existing polytypic phase region. Note that the decay time of a polytypic phase transition can vary in a wide range depending on the exact phase mixing. For instance, in the case of InP nanowires, the decay time of the polytypic transition has been shown to vary from 3.8 ns to more than 13 ns.[43]

To further optimize the GaP passivation, the impact of the shell thickness was investigated. A series of GaAs$_{0.72}$P$_{0.28}$/GaP core/shell NWs with various shell thicknesses: 0, 2.8, 5.6, 8.4, and 14 nm was analyzed. From the above discussion (sample-CS4), the 5.6 nm-thick GaP shell was obtained by depositing GaP for 2 min. Based on this shell thickness and shell deposition time relation, shell thicknesses for other samples in the series were deduced.
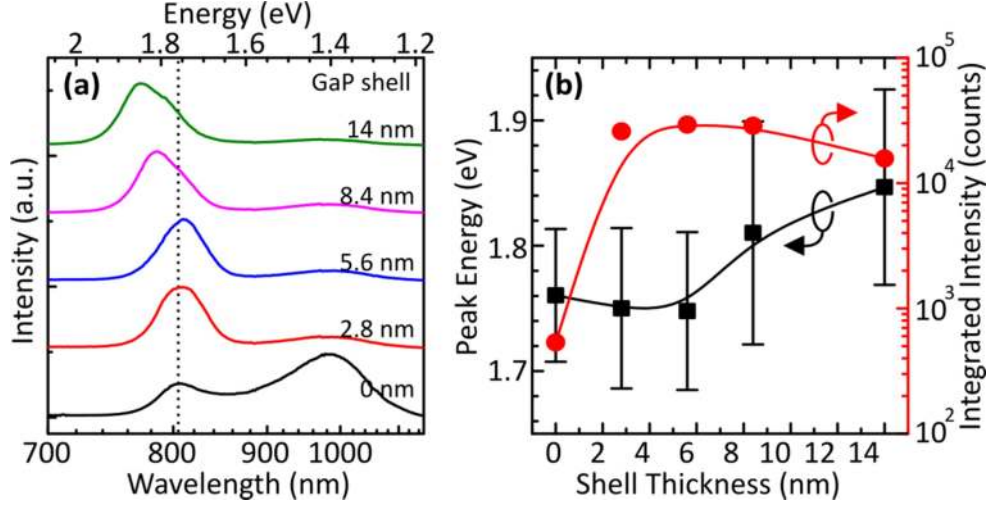
FIG 6. (a) Normalized RT PL spectra of $GaAs_{0.72}P_{0.28}$/GaP core/shell NW ensembles with a different GaP shell thickness, namely 0, 2.8, 5.6, 8.4, and 14 nm. (b) Peak energy and integrated intensity of $GaAs_{0.72}P_{0.28}$/GaP core/shell NW PL spectra versus the shell thickness (error bars represent the full width at half maximum of the NW emission, curves are guides to the eye).

Figure 6(a) shows RT PL spectra of NW ensembles from this sample series. For non-passivated $GaAs_{0.72}P_{0.28}$ NWs (0-nm shell), the sub–band gap luminescence, (broad band centered at 1.4 eV), coming from the parasitic overgrowth on the substrate is dominant. Whereas for the passivated samples (2.8-nm to 14-nm shells), the near band edge luminescence of $GaAs_{0.72}P_{0.28}$ NWs is dominant. The evolutions of integrated intensity, peak energy, and full width at half maximum (FWHM) of all samples are plotted in Fig. 6(b) versus the shell thickness.

For thinner shells, the peak energies red-shift (by 5 meV for 2.8-nm shell, and by 10 meV for 5.6-nm shell), while the integrated intensities increase (by 50 times for 2.8-nm shell, and by 55 times for 5.6-nm shell) in comparison with the bare $GaAs_{0.72}P_{0.28}$ core PL characteristics. For thicker shells, the peak emission spectra blue-shift (by 50 meV for 8.4-nm shell, and by 90 meV for 14-nm shell), while the integrated intensities increase (by 53 times for 8.4-nm shell, and by 29 times for 14-nm shell) in reference to the bare $GaAs_{0.72}P_{0.28}$ core. As seen, the integrated intensities progressively degrade from that of the 5.6-nm shell, accompanied by a spectral broadening (from 126 to 178 meV). The degradation of the integrated intensity, which occurs along with the peak blue-shifting and with the progressive

18

linewidth broadening can be associated with a plastic relaxation of the GaP shell when it exceeds the critical thickness. The sample yielding the highest luminescence intensity has a 5.6 nm-thick GaP shell.

4. Conclusion

In conclusion, we have synthesized by MBE GaAsP NWs possessing high quality zinc-blende structure. The P content was adjusted to ~30%, as evidenced by chemical (EDX) and optical (PL, and CL) analyses, to match the optimal band gap value for tandem III-V/Si solar cells. We have discovered that during the GaAsP core synthesis, the NW was grown by both vapor-liquid-solid (VLS) and vapor-solid (VS) mechanisms, resulting in the formation of an unintentional GaAsP shell which impacts on the optical properties. In-situ surface passivation was investigated by overgrowing the core NWs with Ga(As)P shells of different compositions and thicknesses. The best optical properties are obtained with a GaP shell of moderate thickness (5.6 nm) which prevents plastic relaxation of the radial heterostructure: in comparison with the luminescence characteristics of shell-free GaAsP NWs, the integrated PL intensity is enhanced by two orders of magnitude and the PL decay is more than 20 times longer. Shell of intermediate composition is shown to be less efficient. The calibration of their P concentration contrasts with that of the core region because of the distinct growth mechanisms (VLS for the core and VS for the shell).

References

1. Green, M. A. *et al.* Solar cell efficiency tables (version 50). *Progress in Photovoltaics: Research and Applications* **25,** 668–676 (2017).

2. Glas, F. Critical dimensions for the plastic relaxation of strained axial heterostructures in free-standing nanowires. *Physical Review B* **74,** (2006).

3. Hu, Y., LaPierre, R. R., Li, M., Chen, K. & He, J.-J. Optical characteristics of GaAs nanowire solar cells. *Journal of Applied Physics* **112,** 104311 (2012).

4. Heiss, M. *et al.* III–V nanowire arrays: growth and light interaction. *Nanotechnology* **25,** 014015 (2014).

5. Wallentin, J. *et al.* InP Nanowire Array Solar Cells Achieving 13.8% Efficiency by Exceeding the Ray Optics Limit. *Science* **339,** 1057–1060 (2013).

6. Aberg, I. *et al.* A GaAs Nanowire Array Solar Cell With 15.3% Efficiency at 1 Sun. *IEEE Journal of Photovoltaics* **6,** 185–190 (2016).

7. van Dam, D. *et al.* High-Efficiency Nanowire Solar Cells with Omnidirectionally Enhanced Absorption Due to Self-Aligned Indium–Tin–Oxide Mie Scatterers. *ACS Nano* **10,** 11414–11419 (2016).

8. LaPierre, R. R. Theoretical conversion efficiency of a two-junction III-V nanowire on Si solar cell. *Journal of Applied Physics* **110,** 014310 (2011).

9. Fakhr, A., Haddara, Y. M. & LaPierre, R. R. Dependence of InGaP nanowire morphology and structure on molecular beam epitaxy growth conditions. *Nanotechnology* **21,** 165601 (2010).

10. Wang, Y., Zhang, Y., Zhang, D., He, S. & Li, X. Design High-Efficiency III–V Nanowire/Si Two-Junction Solar Cell. *Nanoscale Research Letters* **10,** (2015).

11. Zhang, Y. *et al.* Self-Catalyzed GaAsP Nanowires Grown on Silicon Substrates by Solid-Source Molecular Beam Epitaxy. *Nano Letters* **13,** 3897–3902 (2013).

12. Holm, J. V. *et al.* Surface-passivated GaAsP single-nanowire solar cells exceeding 10% efficiency grown on silicon. *Nature Communications* **4,** 1498 (2013).

13. Metaferia, W. *et al.* GaAsP Nanowires Grown by Aerotaxy. *Nano Letters* **16,** 5701–5707 (2016).

14. Lloyd-Hughes, J. *et al.* Influence of surface passivation on ultrafast carrier dynamics and terahertz

radiation generation in GaAs. *Applied Physics Letters* **89,** 232102 (2006).

15. Joyce, H. J. *et al.* Electronic properties of GaAs, InAs and InP nanowires studied by terahertz spectroscopy. *Nanotechnology* **24,** 214006 (2013).

16. Haggren, T. *et al.* Strong surface passivation of GaAs nanowires with ultrathin InP and GaP capping layers. *Applied Physics Letters* **105,** 033114 (2014).

17. Couto, O. D. D. *et al.* Effect of a GaAsP Shell on the Optical Properties of Self-Catalyzed GaAs Nanowires Grown on Silicon. *Nano Letters* **12,** 5269–5274 (2012).

18. Demichel, O., Heiss, M., Bleuse, J., Mariette, H. & Fontcuberta i Morral, A. Impact of surfaces on the optical properties of GaAs nanowires. *Applied Physics Letters* **97,** 201907 (2010).

19. Chang, C.-C. *et al.* Electrical and Optical Characterization of Surface Passivation in GaAs Nanowires. *Nano Letters* **12,** 4484–4489 (2012).

20. Matteini, F., Tütüncüoglu, G., Potts, H., Jabeen, F. & Fontcuberta i Morral, A. Wetting of Ga on SiO$_x$ and Its Impact on GaAs Nanowire Growth. *Crystal Growth & Design* **15,** 3105–3109 (2015).

21. Morkötter, S. *et al.* Demonstration of Confined Electron Gas and Steep-Slope Behavior in Delta-Doped GaAs-AlGaAs Core–Shell Nanowire Transistors. *Nano Letters* **15,** 3295–3302 (2015).

22. Colombo, C., Heiβ, M., Grätzel, M. & Fontcuberta i Morral, A. Gallium arsenide p-i-n radial structures for photovoltaic applications. *Applied Physics Letters* **94,** 173108 (2009).

23. Sartel, C., Dheeraj, D. L., Jabeen, F. & Harmand, J. C. Effect of arsenic species on the kinetics of GaAs nanowires growth by molecular beam epitaxy. *Journal of Crystal Growth* **312,** 2073–2077 (2010).

24. www.attolight.com.

25. Rieger, T., Heiderich, S., Lenk, S., Lepsa, M. I. & Grützmacher, D. Ga-assisted MBE growth of GaAs nanowires using thin HSQ layer. *Journal of Crystal Growth* **353,** 39–46 (2012).

26. Priante, G. *et al.* Sharpening the Interfaces of Axial Heterostructures in Self-Catalyzed AlGaAs Nanowires: Experiment and Theory. *Nano Letters* **16,** 1917–1924 (2016).

27. Krogstrup, P. *et al.* Impact of the Liquid Phase Shape on the Structure of III-V Nanowires. *Physical Review Letters* **106,** (2011).

28. Yu, X. *et al.* Evidence for Structural Phase Transitions Induced by the Triple Phase Line Shift in Self-Catalyzed GaAs Nanowires. *Nano Letters* **12,** 5436–5442 (2012).

29. Cirlin, G. E. *et al.* Self-catalyzed, pure zincblende GaAs nanowires grown on Si(111) by molecular beam epitaxy. *Physical Review B* **82,** (2010).

30. Heon Kim, Y., Woo Park, D. & Jun Lee, S. Gallium-droplet behaviors of self-catalyzed GaAs nanowires: A transmission electron microscopy study. *Applied Physics Letters* **100,** 033117 (2012).

31. Plissard, S. *et al.* Gold-free growth of GaAs nanowires on silicon: arrays and polytypism. *Nanotechnology* **21,** 385602 (2010).

32. Jacobsson, D. *et al.* Interface dynamics and crystal phase switching in GaAs nanowires. *Nature* **531,** 317–322 (2016).

33. Vurgaftman, I., Meyer, J. R. & Ram-Mohan, L. R. Band parameters for III–V compound semiconductors and their alloys. *Journal of Applied Physics* **89,** 5815 (2001).

34. Nelson, R. J., Holonyak, N. & Groves, W. O. Free-exciton transitions in the optical absorption spectra of Ga As 1 − x P x. *Physical Review B* **13,** 5415–5419 (1976).

35. Shu-Dong, W. *et al.* Incorporation Behaviour of Arsenic and Phosphorus in GaAsP/GaAs Grown by Solid Source Molecular Beam Epitaxy with a GaP Decomposition Source. *Chinese Physics Letters* **22,** 960–962 (2005).

36. LaPierre, R. R., Robinson, B. J. & Thompson, D. A. Group V incorporation in InGaAsP grown on InP by gas source molecular beam epitaxy. *Journal of Applied Physics* **79,** 3021–3027 (1996).

37. Hou, H. Q., Liang, B. W., Chin, T. P. & Tu, C. W. *In situ* determination of phosphorus composition in GaAs $_{1-x}$ P $_x$ grown by gas-source molecular beam epitaxy. *Applied Physics Letters* **59,** 292–294 (1991).

38. Mancini, L. *et al.* Three-dimensional nanoscale study of Al segregation and quantum dot formation in GaAs/AlGaAs core-shell nanowires. *Applied Physics Letters* **105,** 243106 (2014).

39. Sköld, N. *et al.* Phase Segregation in AlInP Shells on GaAs Nanowires. *Nano Letters* **6,** 2743–2747 (2006).

40. Wagner, J. B., Sköld, N., Reine Wallenberg, L. & Samuelson, L. Growth and segregation of GaAs–AlxIn1−xP core-shell nanowires. *Journal of Crystal Growth* **312,** 1755–1760 (2010).

41. Zhang, Y. *et al.* GaAsP nanowires and nanowire devices grown on silicon substrates. in (ed. Razeghi, M.) 101110X (2017). doi:10.1117/12.2250588

42. Pistol, M.-E. & Pryor, C. E. Band structure of core-shell semiconductor nanowires. *Physical Review*

B **78,** (2008).

43. Akopian, N., Patriarche, G., Liu, L., Harmand, J.-C. & Zwiller, V. Crystal Phase Quantum Dots. *Nano Letters* **10,** 1198–1201 (2010).